Eur. Phys. J. C 12, 369–374 (2000)
Digital Object Identifier (DOI) 10.1007/s100529900233

THE EUROPEAN PHYSICAL JOURNAL C

Study of the QED processes $e^+e^- \to e^+e^-\gamma, e^+e^-\gamma\gamma$ with the SND detector at VEPP-2M

M.N. Achasov, S.E. Baru, A.V. Bozhenok, A.D. Bukin, D.A. Bukin, S.V. Burdin, T.V. Dimova[a], S.I. Dolinsky, V.P. Druzhinin, M.S. Dubrovin, I.A. Gaponenko, V.B. Golubev, V.N. Ivanchenko, A.A. Korol, S.V. Koshuba, A.P. Lysenko, I.N. Nesterenko, E.V. Pakhtusova, S.I. Serednyakov, V.V. Shary, Yu.M. Shatunov, V.A. Sidorov, Z.K. Silagadze, Yu.V. Usov

Budker Institute of Nuclear Physics, Novosibirsk State University, 630090, Novosibirsk, Russia

Received: 20 April / Revised version: 23 August 1999 / Published online: 10 December 1999

Abstract. Results of the SND experiment at the VEPP-2M e^+e^- collider on the QED processes $e^+e^- \to e^+e^-\gamma$ and $e^+e^- \to e^+e^-\gamma\gamma$ with production at large angles are presented. The energy and angular distributions of the final particles were studied. No deviations from QED were found, with an accuracy of 3.8% for the first process and 10.3% for the second.

1 Introduction

Quantum electrodynamics (QED) describes the electromagnetic interactions between electrons and photons with a high accuracy. QED is usually tested in different types of experiments, for example:

(1) high accuracy ($\leq 10^{-6}$) experiments where high order QED corrections at small momentum transfer are tested, for example the anomalous magnetic moments of leptons, the Lamb shift, etc.;
(2) experiments with e^+e^- colliding beams where QED is tested at large momentum transfer, for example:
- $e^+e^- \to \gamma\gamma(\gamma\ldots)$,
- $e^+e^- \to e^+e^-(\gamma,\gamma\gamma\ldots)$,
- $e^+e^- \to \mu^+\mu^-(\gamma\ldots)$,
- $e^+e^- \to \tau^+\tau^-(\gamma\ldots)$.

This work is devoted to the study of the following QED processes with large angles between all particles:

$$e^+e^- \to e^+e^-\gamma, \quad (1)$$

$$e^+e^- \to e^+e^-\gamma\gamma. \quad (2)$$

This study is important for several reasons. First, to check QED: the cross sections and differential distributions can be precisely calculated and compared with the observed ones. Second, possible hypothetical leptons, for example heavy (or excited) electrons [1] (the existence of such a particle is ruled out by recent LEP measurements: $m_{e^*} > 85$–$91\,\mathrm{GeV}$ [2]), can make themselves manifest in the invariant mass spectra of the final particles. Third, these processes could be a source of background for the vector meson decays with electrons and photons in the final state. For example, the process (2) is the background in the study of decays of $\phi \to \eta e^+e^-$, $\eta \to 2\gamma$ and $\phi \to \eta\gamma$, $\eta \to e^+e^-\gamma$. And finally, it is necessary to take into account the process (1) for the luminosity measurements with accuracy $\sim 1\%$.

The processes (1) and (2) were studied in different experiments in different energy regions. Some of these experiments are listed in Table 1.

Table 1. List of some experiments where the processes (1) and (2) were studied

Experiment	$E_{\mathrm{c.m.}}$(GeV)	No. of events
$e^+e^- \to e^+e^-\gamma$		
OLYA [3]	0.6-1.4	1983
ADONE(WAD) [4]	1.9-2.9	99
CELLO [5]	14-46.8	934
JADE [6]	34.4	3227
$e^+e^- \to e^+e^-\gamma\gamma$		
ND [7]	0.6-1.4	223
JADE [6]	34.4	176

2 Detector and experiment

The experiment [8,9] was carried out with the SND detector (Fig. 1) at the VEPP-2M collider [11] in the energy region of the ϕ meson resonance $2E = 0.985$–$1.04\,\mathrm{GeV}$. The SND [12] detector is a general purpose nonmagnetic detector with solid angle coverage $\sim 90\%$ of 4π. It consists of a spherical 3 layer calorimeter based on NaI(Tl) crystals, two drift chambers and a muon system. The list of the SND main parameters is shown in Table 2. The data were recorded in six successive scans at 14 different

[a] Corresponding author, e-mail: baiert@inp.nsk.su

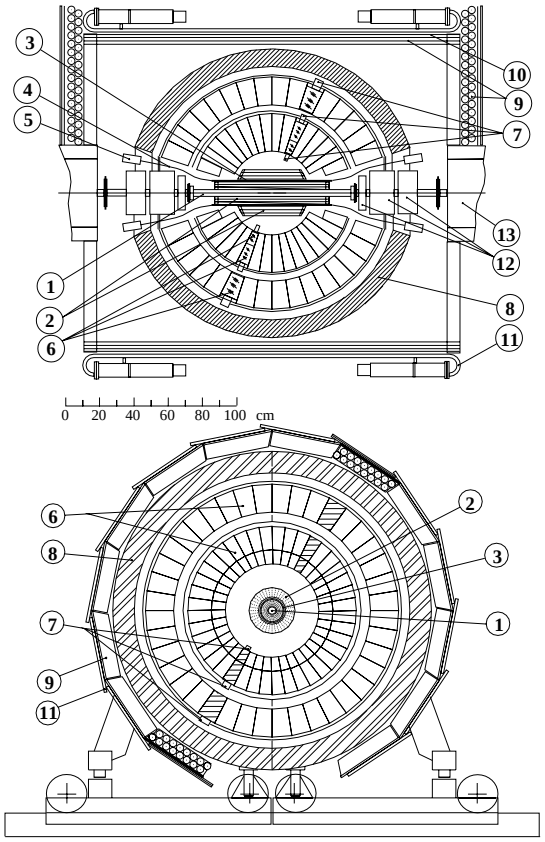

Fig. 1. SND detector: (1) beam pipe, (2) drift chambers, (3) scintillation counter, (4) light guides, (5) PMTs, (6) NaI(Tl) crystals, (7) vacuum phototriodes, (8) iron absorber, (9) streamer tubes, (10) 1 cm iron plates, (11) scintillation counters, (12) and (13) collider magnets

values of the beam energy with the integrated luminosity $\Delta L = 4.1\,\mathrm{pb}^{-1}$. The accuracy of the luminosity determination [9] is estimated to be 3%.

3 Simulation

A Monte Carlo simulation was used for a comparison of the experimental results with the theoretical predictions. A full simulation of the detector was made on the base of the UNIMOD2 program [13]. The process (1) was simulated according to formulae of the order of α^3 from [15]. The details of the implementation of these formulae into the event generator program are described in [14].

For the process (2) formulae of the order of α^4 of the differential cross section, calculated with the method of helicity amplitudes [17] were used. These formulae are valid when all angles between the final particles are large. So the simulation was performed under the condition that all angles are larger than 15°.

The radiative correction for the process (1) was calculated using formulae from [16]. The corrected cross section can be written as $\sigma_{\mathrm{th}} = \sigma_B(1+\delta)$, where σ_{B} is the α^3 Born cross section and δ the calculated radiative correction. The radiation of virtual and soft photons as well as hard photon emission close to the direction of motion of one of the initial or final charged particles were taken into account. These formulae were integrated over phase space as close as possible to the experimental acceptance. The decrease in the registration efficiency due to lost radiative photons was taken into account in the calculation of the contribution from hard photon radiation. As a result $\delta = -(10 \pm 3)\%$ was obtained. The error originates from two main sources: the formula for the differential cross section of virtual and soft photon radiation corrections is incomplete ($\sim 3\%$); the other source of error is the estimation of the efficiency dependence due to the loss of radiative photons ($\sim 1\%$).

Table 2. List of SND parameters

Calorimeter:	
Total number of NaI(Tl) counters	1632
Angular size of the counter	$\Delta\varphi = \Delta\vartheta = 9°$
Read-out	vacuum phototriodes
Noise per counter	$\sim 0.3\,\mathrm{MeV}$
Energy deposition from γs ΔE_γ	$(0.91 \pm 0.02)E_0$ ($E_\gamma = 50$–$700\,\mathrm{MeV}$)
Energy resolution for γs [10] $\sigma E_\gamma/E_\gamma$	$4.2\%/(E(\mathrm{GeV}))^{1/4}$
Angular resolution for γs	$\delta\varphi = \delta\vartheta = 1.5°$ ($E_\gamma = 300\,\mathrm{MeV}$)
Minimal spatial angle for two photons separation	$\Delta\varphi \sim \Delta\vartheta \sim 18°$
Drift chambers:	
Spatial resolution for tracks (P=300 MeV/c)	$\sigma_\varphi = 0.3°$, $\sigma_\vartheta = 2.5°$
Minimal azimuth angle for charged particles separation	$\Delta\varphi \sim 18°$
Amount of material before the chamber	$0.27\ g/cm^2$
Probability of γ conversion before the chamber	0.57%

4 Data analysis

At the first stage of the data analysis the following selection criteria, common to the two processes, were applied:

(1) the number of charged particles $N_{\mathrm{cp}} = 2$;
(2) the number of photons $1 \le N_\gamma \le 3$;
(3) both tracks originate from the interaction region: the distance between tracks and beam axis in the R–ϕ plane $R_{1,2} < 0.5\,\mathrm{cm}$, the Z coordinate of the point on the track closest to the beam axis $|Z_{1,2}| < 10\,\mathrm{cm}$;
(4) the polar angles of all particles $36° < \theta < 144°$;
(5) the acollinearity angle of charged particles in the plane transverse to the beam axis is $|\Delta\phi_{ee}| = |180° - |\phi_1 - \phi_2|| > 5°$;

Table 3. Number of events which passed the selection criteria for $e^+e^- \to e^+e^-\gamma$ and background processes

Process	Number of events	Detection efficiency (%)	Visible cross section
$e^+e^-\gamma$(Exp)	73692		17.9±0.1 nb
$e^+e^-\gamma$(MC)	6081	59.8±1.0	19.7± 0.3 nb
$\omega\pi^0$(MC)	1	0.0033	∼ 0.0003 nb
$\pi^+\pi^-\pi^0$(MC)	556	0.19	∼ 0.02 nb
$\pi^+\pi^-\gamma$(MC)	8	0.08	∼ 0.05 nb

(6) the normalized total energy deposition $E_{\rm tot}/2E_0 > 0.8$;
(7) the normalized total momentum$P_{\rm tot}/E_{\rm tot} < 0.15$;
(8) the minimal energy of a charged particle is $E_{e\ \rm min} > 10$ MeV;
(9) the minimal energy of a photon is $E_{\gamma\ min} > 20$ MeV;
(10) no hits in the muon system.

Nearly 90,000 events passed these cuts for use in the further analysis.

4.1 The process $e^+e^- \to e^+e^-\gamma$

For the selection of events from the process (1) a kinematic fit imposing 4-momentum conservation was applied. The parameter χ^2, describing the degree of energy-momentum balance in the event, was calculated. For the selection of events from the process $e^+e^- \to e^+e^-\gamma$ an additional cut was imposed: $\chi^2 < 15$.

The number of events thus selected in the experiment and in the simulation of the process (1) as well as for some background processes are shown in Table 3.

The corresponding energy and the angular and invariant mass distributions after a kinematic fit are shown in Figs. 2 and 3. The statistical errors in these figures are comparable with the marker size. The peaks in Fig. 2a,b,c originate from quasi-elastic events of the process (1) with radiation of a soft photon with energy $E_\gamma/E_0 \ll 1$. There is good agreement between the experimental data and the MC simulation. There are no traces of heavy leptons in the invariant mass spectrum in Fig. 3c. Some minor differences in the spectra (Figs. 2d, 3a) could be attributed to the imprecise simulation of the angular differential nonlinearity for photons caused by granularity of the calorimeter.

The estimated detection efficiency for the described selection criteria is equal to $59.8 \pm 1.0\%$ (the error is statistical). It was defined with respect to simulation under the following conditions: the polar angle of final particles was $36^\circ < \theta < 144^\circ$, the azimuth acollinearity angle was $\Delta\phi_{ee} > 5^\circ$, the spatial angle between the final particles is $\theta_{ee,e\gamma} > 20^\circ$; the minimal energies for the charged particles and photons are equal to 10 and 20 MeV, respectively. The systematic error of the measured cross section is determined by the normalization uncertainty (3%), the

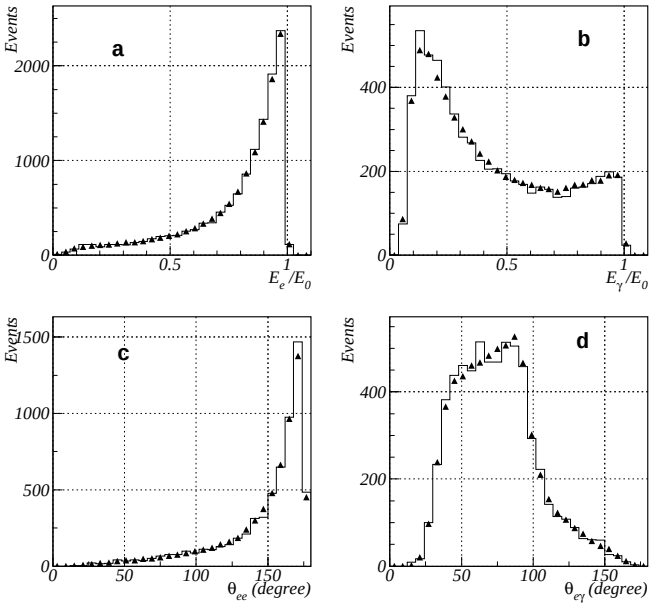

Fig. 2. Energy and angular spectra for the process $e^+e^- \to e^+e^-\gamma$: **a** energy spectrum of the charged particles; **b** the energy spectrum of the photons; **c** the angle between the charged particles; **d** the minimal angle between a charged particle and a photon; ▲: experimental points; histogram: simulation

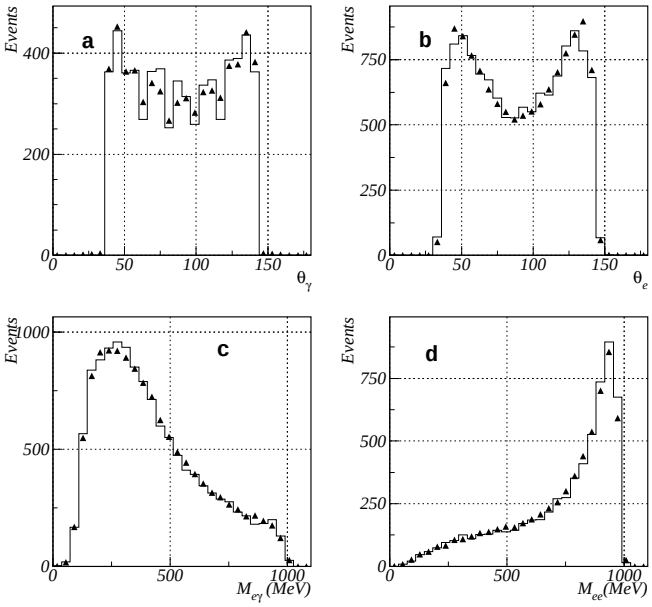

Fig. 3. Angular and invariant mass spectra for the process $e^+e^- \to e^+e^-\gamma$: **a** the polar angle of the photons; **b** the polar angle of the charged particles; **c** the invariant mass of a pair consisting of a charged particle plus a photon; **d** invariant mass of the charged particles; ▲: experimental points; histogram: simulation

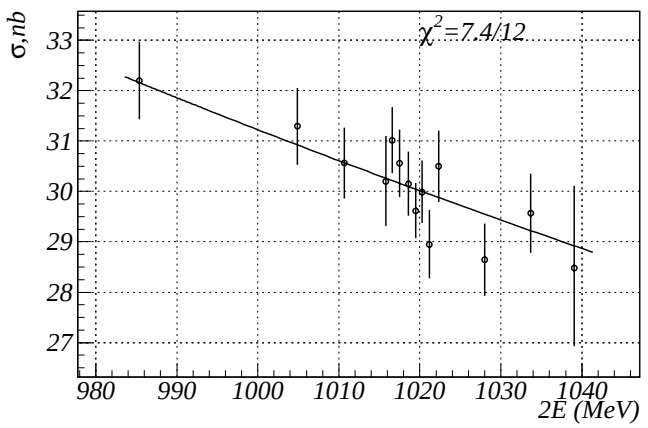

Fig. 4. Cross section energy dependence for the process $e^+e^- \to e^+e^-\gamma$. Points are for the experiment, a line is a fit with formula (3)

limited MC statistics (1.7%) and the uncertainties in the selection efficiency (1.5%). In total it is equal to 3.8%.

The energy dependence of the cross section of the process (1) is shown in Fig. 4. The measurements were fitted using the following function:

$$\sigma(E) = \sigma_0(E) \cdot (E_0^2/E^2) + W \cdot \sigma_\phi(E), \qquad (3)$$

where the first term has the energy dependence typical of QED processes and the second corresponds to a contribution from ϕ meson decays with a cross section σ_ϕ. The fitting parameters are σ_0, the cross section at the energy $E_0 = 1020\,\mathrm{MeV}$, and W, which determines the resonance background contribution. The main part of this background for the process (1) comes from the $\phi \to \pi^+\pi^-\pi^0$ decay.

Fitting gives no peak from the ϕ meson decays (Fig. 4). The fitted experimental cross section is $\sigma_0 = 30.01 \pm 0.12 \pm 1.2\,\mathrm{nb}$ and the expected QED cross section with radiative corrections is $\sigma_{\mathrm{th}} = 29.7 \pm 0.3 \pm 1.0\,\mathrm{nb}$. The observed difference ($\sim 1\%$) is within the systematic error.

4.2 The process $e^+e^- \to e^+e^-\gamma\gamma$

For the selection of events from the process $e^+e^- \to e^+e^-\gamma\gamma$, the following additional cuts were imposed:

(1) the number of photons is $2 \le N_\gamma \le 3$;
(2) $\chi^2 < 15$;
(3) to suppress the contribution from $e^+e^- \to \pi^+\pi^-\pi^0$ the region $110 < M_{\gamma\gamma} < 170\,\mathrm{MeV}$ was excluded;
(4) the minimal energy of the photons is $E_{\gamma\ \mathrm{min}} = 50\,\mathrm{MeV}$.

Here χ^2 is the kinematic fit parameter obtained under the assumption that the events come from the process (2). The number of events which passed these selection criteria in the experiment and in the Monte Carlo simulation of the process (2) and the background processes are shown in Table 4.

The energy and the angular and invariant mass distributions, after a kinematic fit are shown in Figs. 5 and 6. Similar to the process (1) the peaks are seen from quasi-elastic scattering with the emission of soft photons (Fig. 5a,b,c). The peak in the photon energy spectra (Fig. 5b) near $E_\gamma/E_0 = 0.7$ corresponds to the recoil photon energy in radiative decays: $\phi \to \eta\gamma$, $\eta \to e^+e^-\gamma$, $\pi^+\pi^-\gamma$. Some enhancement in the two photon invariant mass spectrum (Fig. 6b) near the η mass appears from the decay $\phi \to \eta e^+e^-, \eta \to \gamma\gamma$. There are also no visible traces of heavy lepton production in the $M_{e\gamma}$ spectrum (Fig. 6d).

The detection efficiency was determined from a simulation under nearly the same conditions as for the process (1): the polar angle of the final particles is $36° < \theta < 144°$, the azimuth acollinearity angle is $\Delta\phi_{ee} > 5°$, the spatial angle between the final particles is $\theta_{ee,e\gamma,\gamma\gamma} > 20°$, the

Table 4. The number of events which passed the selection criteria for $e^+e^- \to e^+e^-\gamma\gamma$ and background processes

Process	Number of events	Detection efficiency (%)	Visible cross section (nb)
$e^+e^-\gamma\gamma$ (Exp.)	698		0.153 ± 0.013
$e^+e^-\gamma\gamma$ (MC)	647	33.6 ± 1.5	0.151 ± 0.006
$\omega\pi^0$ (MC)	3	0.01	~ 0.001
$\pi^+\pi^-\pi^0$ (MC)	16	0.006	~ 0.0006
$\pi^+\pi^-\gamma$ (MC)	1	0.001	~ 0.001

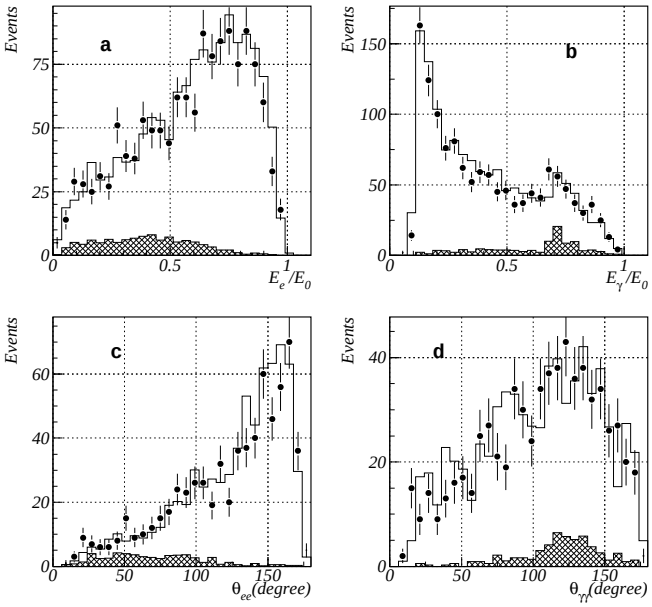

Fig. 5. Energy and angular spectra for the process $e^+e^- \to e^+e^-\gamma\gamma$: **a** the energy spectrum of the charged particles; **b** the energy spectrum of the photons; **c** the angle between the charged particles; **d** the angle between the photons; •: experimental points; filled histogram: simulation of background from the Dalitz decays $\phi \to \eta e^+e^-, \eta \to \gamma\gamma$ and $\phi \to \eta\gamma, \eta \to e^+e^-\gamma$; histogram: sum of simulations of QED process and background

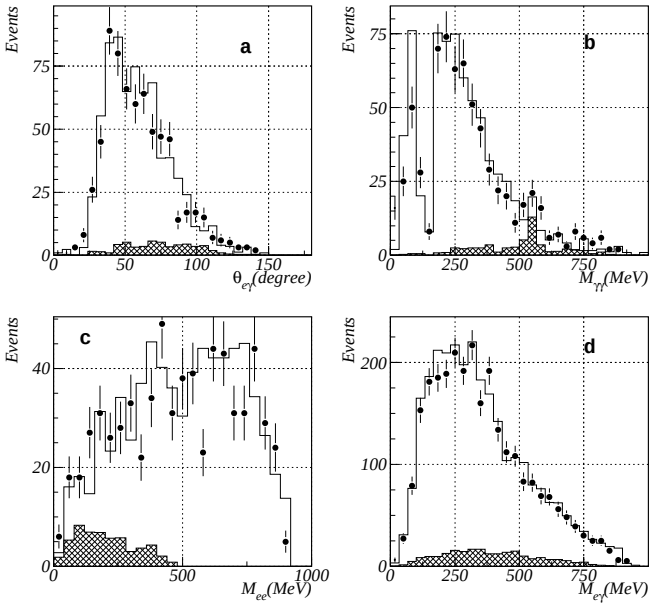

Fig. 6. Angular and invariant mass spectra for the process $e^+e^- \to e^+e^-\gamma\gamma$: **a** the minimal angle between the charged particles and the photons; **b** the invariant mass of two photons; **c** the invariant mass of the charged particles; **d** the invariant mass of a pair consisting of a charged particle and a photon; •: experimental point; filled histogram: simulation of background from Dalitz decays $\phi \to \eta e^+e^-$, $\eta \to \gamma\gamma$ and $\phi \to \eta\gamma, \eta \to e^+e^-\gamma$; histogram: sum of simulations of QED process and background

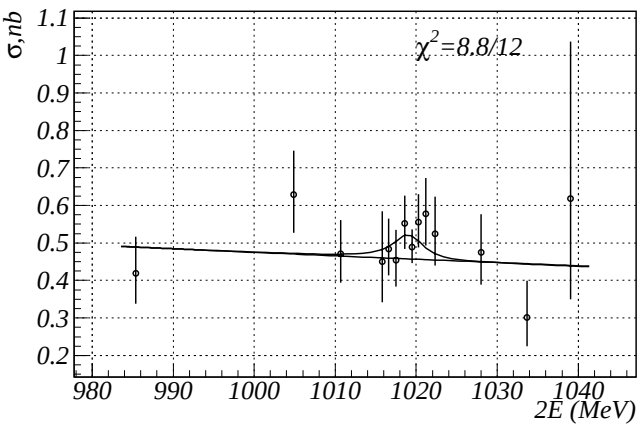

Fig. 7. The cross section energy dependence for the process $e^+e^- \to e^+e^-\gamma\gamma$. Points: experiment; a line: fit with formula (3)

Table 5. Number of events and experimental cross section for $e^+e^- \to e^+e^-\gamma$

$E_{\rm c.m.}$(MeV)	No. of events	Experimental cross section (nb)
985.4	3827	19.26
1004.9	3545	18.71
1010.7	4616	18.27
1015.8	2150	18.06
1016.6	5811	18.54
1017.5	5506	18.27
1018.6	7492	18.03
1019.5	19049	17.71
1020.3	7395	17.93
1021.2	4550	17.31
1022.3	4138	18.24
1028.0	3436	17.13
1033.7	2792	17.67
1039.1	410	17.03

minimal energies for the charged particles and photons are equal to 10 and 50 MeV, respectively. The value of the detection efficiency was found to be 33.6± 1.5%.

The fitting of the energy dependence of the cross section of the process (2) was done using (3). The result is shown in Fig. 7. The contribution from the ϕ decays is seen as a peak at the ϕ mass. The significance of the peak is ~ 1.5 of the standard deviation. The processes $\phi \to \eta e^+e^-, \eta \to \gamma\gamma$ and $\phi \to \eta\gamma, \eta \to e^+e^-\gamma$, mentioned above, constitute the main contribution to the peak. The fitted value of the experimental cross section $\sigma_0 = 0.457 \pm 0.039 \pm 0.026$ nb was found to be in good agreement with the calculated QED cross section $\sigma_{\rm MC} = 0.458 \pm 0.010$ nb. The systematic error included in σ_0 is determined by the normalization uncertainty (3%), the limited MC statistics (4.5%) and the uncertainties on the selection efficiency (2.%). In total it is equal to 5.8%.

5 Conclusions

In the experiment with the SND detector at the VEPP-2M collider the $e^+e^- \to e^+e^-\gamma$ and $e^+e^- \to e^+e^-\gamma\gamma$ QED processes with particles produced at large angles were studied. A total of 73,692 events of the process $e^+e^- \to e^+e^-\gamma$ was observed. For the process $e^+e^- \to e^+e^-\gamma\gamma$ 698 events were observed where 649 events are from the QED process (2). The number of events observed in different energy points for both processes are shown in Tables 5 and 6. The cross sections and differential distributions of the produced particles were compared with an MC simulation. No significant deviations from QED were found within the limits of the measurement errors, which are equal to 3.8% and 10.3% for the processes (1) and (2), respectively.

Acknowledgements. This work was supported in part by the Russian Foundation of Basic Researches (Grant No. 96-15-96327); and STP "Integration" (Grant No. 274).

References

1. F.E. Low, Phys. Rev. Lett. **14**, 238 (1965)
2. C. Caso et al., Eur. Phys. J. C **3**, 775 (1998)
3. A.D. Bukin et al., Sov. J. Nucl. Phys. **35**, 844 (1982)
4. C. Bacci et al., Phys. Lett. B **71**, 227 (1977)

Table 6. Number of events and experimental cross section for $e^+e^- \to e^+e^-\gamma\gamma$ with subtracted ϕ meson background

$E_{\rm c.m.}$(MeV)	No. of events	Experimental cross section (pb)
985.4	28	141.
1004.9	40	210.
1010.7	40	156.
1015.8	17	144.
1016.6	48	153.
1017.5	42	139.
1018.6	68	163.
1019.5	156	145.
1020.3	70	169.
1021.2	48	182.
1022.3	39	170.
1028.0	32	159.
1033.7	16	101.
1039.1	5	208.

5. H.-J. Behrend et al., Phys. Lett. B **158**, 536 (1985)
6. B. Naroska et al., Phys. Rep. **148**, 67 (1987)
7. S.I. Dolinsky et al., Phys. Rep. **202**, 99 (1991)
8. M.N. Achasov et al., Preprint Budker INP 96-47, Novosibirsk, 1996
9. M.N. Achasov et al., Preprint Budker INP 97-78, Novosibirsk, 1997; hep-ex/9710017, October, 1997
10. M.N. Achasov et al., Nucl. Instrum. Meth. A **411**, 337 (1998)
11. G.M. Tumaikin, in Proceedings of the 10th International Conference on High Energy Particle Accelerators, Protvino, **1**, 443 (1977)
12. V.M. Aulchenko et al.,in Proceedings of the Workshop on Physics and Detectors for DAΦNE (INFN, Frascati, Italy 1991), p. 605
13. A.D. Bukin et al., Preprint BINP 90-93, 1992, Novosibirsk; in Proceedings of the Workshop on Detector and Event Simulation in High Energy Physics (NIKHEF, Amsterdam, The Netherlands 1991), p. 79
14. A.D. Bukin, Preprint BINP 85-124, 1985, Novosibirsk
15. V.N. Baier et al., Phys. Rep. **78**, 293 (1981)
16. A.B. Arbuzov, E.A. Kuraev, B.G. Shaikhatdenov, hep-ph/9805308, August 1998
17. E.A. Kuraev, A.N. Peryshkin, Sov. J. Nucl. Phys. **42**, 756 (1985)